Materials Chemistry and Physics xxx (2013) 1–11

Contents lists available at SciVerse ScienceDirect

Materials Chemistry and Physics

journal homepage: www.elsevier.com/locate/matchemphys

Distortion and residual stress measurements of induction hardened AISI 4340 discs

J. Yi [a], M. Gharghouri [b], P. Bocher [c], M. Medraj [a,*]

[a] Department of Mechanical Engineering, Concordia University, 1455 de Maisonneuve Blvd. W. Montreal, Quebec H3G 1M8, Canada
[b] National Research Council Canada, Canadian Neutron Beam Centre, Chalk River Laboratories, Chalk River, Ontario K0J 1J0, Canada
[c] Department of Mechanical Engineering, ETS, 1100 rue Notre-Dame West, Montreal, Quebec H3C 1K3, Canada

HIGHLIGHTS

- Residual stress profiles of induction hardened 4340 steel were obtained using neutron diffraction.
- Effects of induction hardening parameters on hardening depth and distortions were examined.
- Effects of initial hardness on hardening depth and distortions were examined.
- d_0 Depth distribution was investigated by neutron diffraction technique.
- The variation in d_0 can significantly affect the residual stress results.

ARTICLE INFO

Article history:
Received 21 December 2012
Received in revised form
15 May 2013
Accepted 4 July 2013

Keywords:
Metals
Heat treatment
Neutron scattering and diffraction
X-ray scattering
Residual stress

ABSTRACT

10 Induction hardened discs with two initial hardness levels were used for exploring the influences of the variation of initial hardness as well as induction hardening (IH) recipes on the heat treatment distortions and hardening depth. The results show that for the same initial hardness, the larger the energy input, the higher the distortion size as well as the hardening depth. For a given induction hardening recipe, the increase in initial hardness leads to a deeper hardening depth but a smaller distortion. One disc was selected for the residual stress investigation in three orthogonal directions by neutron diffraction (ND). The corresponding stress-free lattice spacing d_0 was measured from the same material using both ND and X-ray diffraction (XRD) methods. The ND results show that the variation of d_0 in the hardened layer is significant and should be taken into account for stress calculation. However, regarding the core region, the d_0 value measured by XRD is more reliable. Accordingly, a combination of the ND-measured d_0 profiles in the hardened layer and the XRD-measured d_0 value in the core was adopted for the determination of residual stress distributions.

1. Introduction

High performance mechanical components used for aerospace applications require high strength, high hardness and satisfactory toughness. In order to meet these requirements, a variety of heat treatments, especially surface hardening techniques, are employed. In recent years, induction hardening (IH) has attracted considerable attention because it provides significant improvements in fatigue strength of the mechanical parts. Moreover, IH treatment can be performed very quickly and it is an environmentally friendly process.

In IH, the work-piece is first heated quickly using an oscillating electromagnetic field, and then quenched to room temperature [1]. Only material at the surface of the work-piece undergoes phase transformation, resulting in a hardened surface layer. The core material maintains a high toughness. The treatment results in compressive stresses at the surface, balanced by tensile stresses in the bulk of the component, which results in improved fatigue performance.

In the past ten years, many researchers have studied the correlation between IH process parameters and the resulting residual stress distributions [2,3]. The distortions associated with the IH treatment have also been studied [4].

X-ray diffraction (XRD) and neutron diffraction (ND) are non-destructive techniques [5,6] widely used in residual stress examination. XRD is a powerful tool for near-surface ($\leq$10 μm [7]) stress measurement, but its low penetration depth makes it hard to determine the residual stress profile in the bulk. By alternately removing

* Corresponding author. Tel.: +1 514 848 2424x3146.
E-mail address: mmedraj@encs.concordia.ca (M. Medraj).

0254-0584/$ – see front matter © 2013 Elsevier B.V. All rights reserved.
http://dx.doi.org/10.1016/j.matchemphys.2013.07.012

material and performing XRD measurements, it is possible to probe the residual stress to depths of several millimeters. However, this technique depends on a stress relaxation correction (usually based on the model given by Moore and Evan in 1958 [8]) which leads to certain uncertainties. These uncertainties have been found to increase significantly with increasing depth. For example, Coupard et al. [9] claimed that the Moore and Evan correction only worked well when the whole removed depths lower than one-tenth of the outside diameter of the disc-shaped sample. For greater depths, a more reliable experimental investigation is required. Accordingly, in the present study, ND was adopted to determine the bulk residual stress profile due to its strong penetration in most engineering materials (maximum 25 mm penetration depth for steel [7,10,11]).

Although many studies of the residual stress and distortions associated with heat treatments have been performed in recent years, an exploration of the correlation between the IH process parameters and their effects on distortions and residual stresses is still needed. This is the purpose of the present study.

The difficulties associated with surface residual stress measurements after various surface treatments have attracted considerable attention. For example, Hutchings et al. [11] and Prevey [12] pointed out that a significant stress gradient in the ND or XRD sampling volume will affect the stress results. Besides, in measuring residual strain by neutron or by X-ray diffraction, it is critical to obtain accurate measurements of the stress-free lattice parameter, d_0. This is because even a small change in d_0 can result in significant changes in the corresponding stress value.

Generally, IH parts exhibit severe hardness variations from the surface to the bulk, due to the changes in microstructure which resulted from the phase transformation. This difference in microstructure can in turn lead to considerable variations in d_0 values at corresponding positions. Therefore, the investigation of d_0 from sample's surface to the core in IH parts is very important. By virtue of specific formula developed, Prevey and Mason [13] calculated the d_0 distribution in the normal direction as a function of depth from the axial and hoop residual stress measured from an IH sample by XRD. Their d_0 profile showed smaller d_0 values at the surface (suggesting some decarburization of the part) and some fluctuations in d_0 in the core material. Ezeilo and Webster [14] measured d_0 at the surface and in the base of a laser surface remelted specimen by neutron diffraction. For the intermediate material, a linear variation of d_0 was used. They calculated the residual stress based on this neutron-measured d_0 and compared it with that obtained by XRD and by thermal-mechanical model. They indicated the importance of applying appropriate values of the stress-free lattice spacing in neutron diffraction stress calculations, if the material under investigation has considerable variation in microstructure.

2. Experimental procedure

2.1. Material and specimen geometry

Samples used in this study were made of AISI 4340 steel. The chemical composition of the specific alloy used is provided in Table 1 [15]. The geometry of the samples is sketched in Fig. 1. It is a 7.0 mm thick hollow disc with outside diameter of 106.1 mm and inside diameter of 13.5 mm prior to induction hardening.

Two batches of five disc samples were prepared. Group I samples had an initial hardness of 43 HRC (423 HV) and group II samples had an initial hardness of 27 HRC (279 HV).

2.2. Induction surface hardening

The aim of induction hardening is to produce a hard surface layer while maintaining the initial hardness (the hardness before induction hardening) in the core. Fig. 2 contains photographs of the induction hardening process used in this work.

Table 1
Chemical composition of steel AISI 4340 [15].

Element	Content (wt %)
C	0.38–0.43
Cr	0.70–0.90
Mn	0.60–0.80
Mo	0.20–0.30
Ni	1.65–2.00
P	0.040max
Si	0.20–0.35
S	0.040max
Fe	Balance

The inductor was a coil with a coupling distance (the gap between the inside radius of the coil and the outside radius of the disc) of 1.5 mm. All samples were induction hardened using a frequency of 200 kHz. The rotation speeds of the part during heating and quenching were 360 rpm and 240 rpm respectively. The heating time and power were varied to generate a range of IH conditions. The disc was firstly quickly heated by the current generated on the surface and then quenched by the Aqua-Quench solution (water + 12% to 12.5% polymer) sprayed from the quenching rig (Fig. 2) to reach room temperature. No additional tempering treatment was applied. Table 2 shows the selected IH parameters for the two batches.

2.3. Distortion measurement

Distortion measurements were conducted on each disc sample using a Mitutoyo Bright-STRATO 7106 coordinate measuring machine (CMM) at room temperature. The probe used in the present study was a ruby ball with a diameter of 1.5 mm. The resolution of this equipment is close to ±0.1 μm and the experimental repeatability was found to be ±0.6 μm.

Variations in the coordinates of points located on the three faces of the disc before and after the IH treatment were measured. As shown in Fig. 3, for the top and bottom faces, distortion measurements were carried out from the OD (outside diameter) to 10 mm towards the center of the disc. For the lateral face, measurements were performed along the thickness of the disc. For all three faces, measurements were performed at 48 equally-spaced circumferential locations as shown in Fig. 3b. Identical measurement locations were used on the top and bottom faces, resulting in 2880 points on each face. Each measuring line comprised 60 measuring points. The spacing in the radial direction between measuring

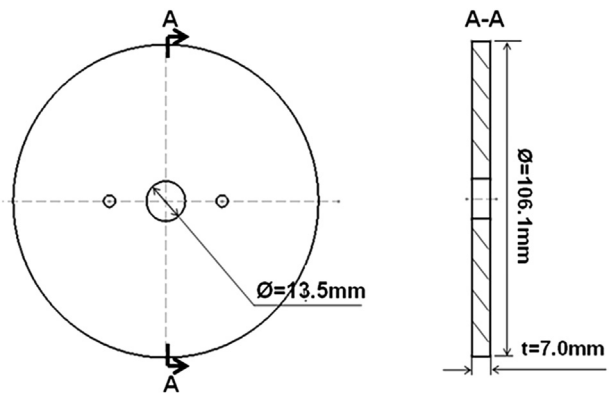

Fig. 1. Specimen geometry (dimensions in mm).

Please cite this article in press as: J. Yi, et al., Distortion and residual stress measurements of induction hardened AISI 4340 discs, Materials Chemistry and Physics (2013), http://dx.doi.org/10.1016/j.matchemphys.2013.07.012

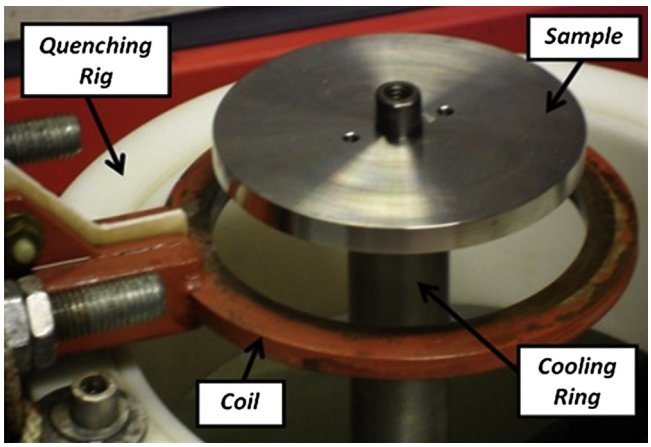

Fig. 2. Photographs of the induction hardening process experimental set-up.

points was 0.1 mm within the hardened layer up to 5 mm in from the circumference. A larger spacing of 0.5 mm was used for the remainder of the measurements. For the lateral face, measurements were performed at 11 points spaced about 0.6 mm apart.

2.4. Residual stress investigation

Neutron diffraction (ND) investigations were carried out on the L3 spectrometer of the Canadian Neutron Beam Centre, National Research Council, Canada. A monochromatic neutron beam was obtained using the {*115*} reflection of a germanium mosaic single crystal at a take-off angle of 98.77°, (λ = 1.653Å). The neutrons' wavelength was determined using four diffraction peaks from a nickel powder standard sample. With this wavelength, the *α-Fe* {*211*} reflection occurred at a scattering angle $2\theta\{112\} = 89.90°$ which, being close to 90°, provided optimal spatial resolution and avoided peak asymmetry arising as a result of axial divergence. The {*211*} reflection was selected for the measurements as it has been shown to be insensitive to inter-granular strains for metals with a body-centered cubic unit cell. A 32-wire based multi-wire detector spanning a scattering angle of 2.54° was used and the specimen was continuously oscillated ±0.5° during data acquisition to ensure that enough grains were sampled.

2.4.1. Stress-free lattice spacing determination

Stress-free lattice spacing (d_0) was obtained from measurements on a notionally stress-free reference sample, a comb produced from an extra disc that had undergone the same IH process which was applied on disc #5 (the disc selected for residual stress investigation by ND). The comb is composed of 40 (0.3 × 0.3 mm^2) teeth Xmm distant apart (Fig. 4).

Measurements were performed on the first 10 teeth of the comb only, along the transverse direction as indicated in Fig. 5. This is because the lattice spacing should not vary significantly beyond this 10-tooth distance (around 5.0 mm), considering the desired thickness of the hardened layer is less than 1.5 mm. The center of the sampling gauge volume (SGV) was located at tooth mid-height and in the center of each investigated tooth.

Table 2
Induction hardening parameters applied on samples.

Sample (initial hardness, HRC)		Induction hardening parameters		
Group I 43HRC (423HV)	Group II 27HRC (279HV)	Power[a] (KW)	Heating time (s)	Quenching medium
Disc#1	Disc#6	80	0.75	Water + (12%–12.5%) polymer (Aqua-Quench solution)
Disc#2	Disc#7	80	0.25	
Disc#3	Disc#8	62	0.25	
Disc#4	Disc#9	62	0.75	
Disc#5	Disc#10	71	0.50	

[a] The mean value.

2.4.2. Residual stress determination

The ND set-up for the targeted sample (disc #5) is shown in Fig. 6. Measurements were carried out at the disc's mid-thickness at a series of locations along the radius, from a depth of approximate 0.2 mm–5.0 mm. The measuring step was 0.1 mm within the depth of 2 mm and was 0.5 mm in the following 3 mm, giving 25 measuring points in total. ND data were acquired for the hoop (*X*), axial (*Z*) and radial (*Y*) directions.

Fig. 7(a)–(c) represents the diffracting volume used for the radial, hoop and axial residual stress measurement in present ND study. The diffracting volume (sampling gauge volume, SGV) was of a rectangular shape: Ymm in the radial direction, Xmm in the hoop direction and Zmm in the axial direction. As shown, the ND-measured lattice strain is the averaged lattice strain over the SGV of the sample, which is decided by the width of the two beam slits (incident and diffraction beam slits) and the gauge height applied. The SGV was 0.36 mm^3 (0.3 × 0.3 × 4) for radial direction and were 2.7 mm^3 (3 × 3 × 0.3) for both hoop and axial directions lattice strain measurements.

2.5. Evaluation of the transformed region

The approximate size of the transformed region of all samples (two batches) was measured by a visual method. Without cutting process, samples were mechanically polished by sandpaper and then etched immediately by Nital liquid on the edges of both top and bottom faces. By virtue of optical microscope, the approximate transformed depth could be seen and measured directly. Because this method is not accurate enough (only for giving an estimated length of hardened layer), the main purpose here is to make a series comparisons among samples. The real transformed region of the hardened sample can be obtained by measuring the hardness profile of the investigated sample.

2.5.1. Micro-hardness measurement

In this study, Vickers micro-hardness test was applied only on the specimen (disc #5) used for residual stress investigation. A small piece was cut from the disc and mounted. The hardness investigation was carried out at ETS by using FUTURE-TECH FM-1 machine with the constant load of 200 g. The measuring step was 0.1 mm in the hardened and transition zones, and 0.5 mm in the non-affected region of the sample. Hardness profile was established along the cross-section (radial direction) at three positions (top-, mid- and bottom-thickness) separately, as illustrated in Fig. 8.

2.5.2. Microstructure investigation

Microstructural analysis was carried out on the cross-section of disc #5. This was performed using a Hitachi S-3400N SEM (Scanning Electron Microscopy).

3. Results and discussions

3.1. Transformed depth results

3.1.1. Transformed depth result of group I

Photographs of the transformed regions after IH for the discs in group I (with initial hardness of 43HRC) are shown in Fig. 9. The images show disc #1 to #5 top and bottom surface edges after etching. The overall hardening depth order is as follow: disc

Please cite this article in press as: J. Yi, et al., Distortion and residual stress measurements of induction hardened AISI 4340 discs, Materials Chemistry and Physics (2013), http://dx.doi.org/10.1016/j.matchemphys.2013.07.012

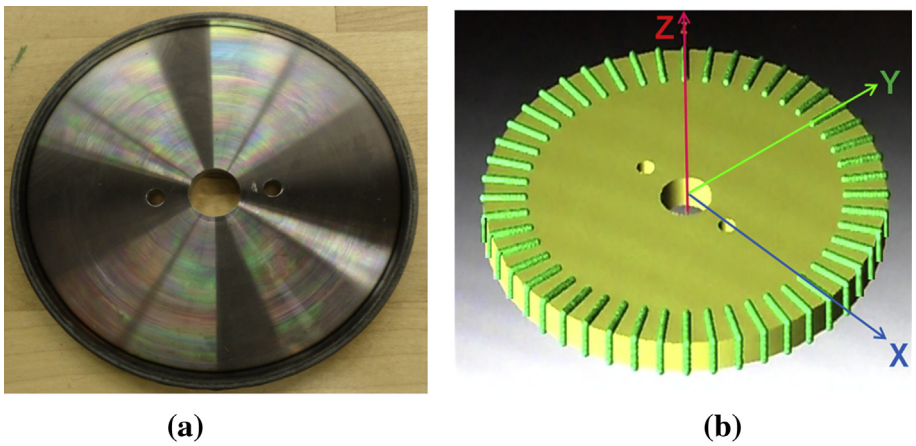

Fig. 3. (a) A photograph of a typical induction hardened sample and (b) schematic diagram of measuring points distributions on each face.

#1 > disc #4 > disc #5 > disc #2 > disc #3 which follows the level of energy input (Table 2) (i.e. longer heating time and/or larger input power). Moreover, it should be noted that all five discs in this group display a similar discrepancy in hardening depth between the top and bottom faces (see Fig. 9). The hardening depth on bottom face is slightly larger than the top one for all cases. Although such discrepancy is relatively small and therefore the hardening depth on the top and bottom faces can be seen as similar, the possible reasons for this discrepancy need to be discussed. Firstly, this hardening depth difference probably suggests that the disc sample was not perfectly centered in the coil before performing the IH process – the disc may be positioned a little higher which makes less intense of the magnetic field at the bottom face. On the other hand, this discrepancy may indicate a non-perfect-flat coil surface. Similar results were obtained for the other group (group II) of discs.

3.1.2. Transformed depth comparison between groups I and II

A comparison of the hardening depths for groups I and II is shown in Fig. 10. It is clearly shows that for the same IH recipe, discs with a higher initial hardness of 43 HRC (423 HV) display a greater hardening depth. The results suggest that in order to obtain the same induction hardening depth, steel samples with a lower initial hardness require more heat input than do steels with a higher initial hardness. This could be due to the fact that for a given composition, the lower hardness steel has a relatively higher austenite transformation temperature according to the relevant phase transformation diagram [16]. The graph in Fig. 10 also shows that the hardening depth increases linearly with increasing input energy.

3.2. Distortion results

3.2.1. Distortion results of group I

Only distortion results for group I (initial hardness of 43 HRC (423 HV)) will be discussed here. Similar trends were observed in group II. Fig. 11(a)–(e) illustrates the dimensional changes of discs #1 to #5 in the axial (left column) and radial (right column) directions. The average hardened depth (HD_{avg}) measured from the top and bottom faces of the corresponding disc are also included for reference. The origin of the coordinate axes was located at the bottom surface of the disc and therefore $Z = 0$ mm and $Z = 7$ mm (approximately) represent the bottom and the top surfaces, respectively, as illustrated in Fig. 8.

The ΔZ profiles on the top and bottom surfaces are approximately symmetric for all samples. The axial distortion patterns are almost the same on these two faces for every disc. For all of the discs, the region close to the disc center shows no significant axial distortion (ΔZ). In contrast, near the periphery of the disc, the distortion becomes significant, showing a convex pattern, as if the materials had undergone some expansion. This could be partly due to the phase transformation at the surface hardened layer due to the induction hardening. If comparing the size (maximum of absolute ΔZ) and range of axial distortions among these five discs, it can be found that the axial distortion sequence yields: disc #1 > disc #4 > disc #5 > disc #2 ≥ disc #3. It is not surprising to note that disc #1 has the largest while disc #3 has the smallest distortion, since they correspond to the strongest (longest heating time with highest input power) and weakest (shortest heating time with smallest input power) IH recipes, respectively.

For the radial distortion (ΔR) profiles, disc #1 has a different radial distortion profile from the other discs and distinctly large

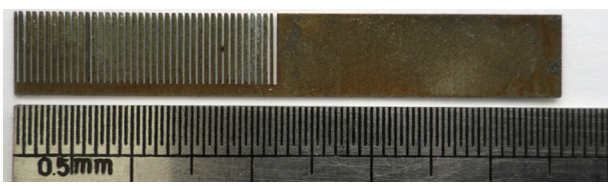

Fig. 4. The stress-free reference comb sample photograph taken after wire-EDM.

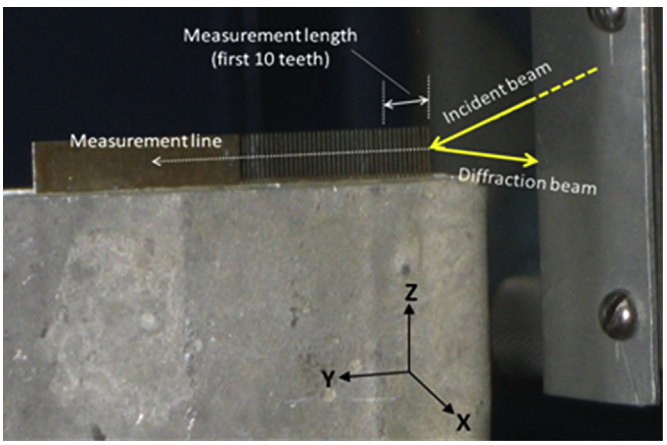

Fig. 5. ND set-up of comb sample for unstressed parameter d_0 investigations.

Please cite this article in press as: J. Yi, et al., Distortion and residual stress measurements of induction hardened AISI 4340 discs, Materials Chemistry and Physics (2013), http://dx.doi.org/10.1016/j.matchemphys.2013.07.012

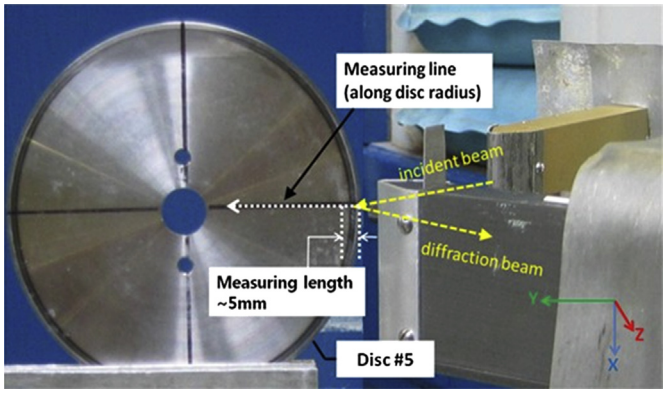

Fig. 6. ND set-up for radial residual strain measurement of the disc.

radial distortion, with ΔR in the range from approximately −0.06 mm to 0.10 mm. It displays two noticeable protuberance patterns at each side. This is consistent with its extraordinary large axial distortions measured on top and bottom faces. In fact, during the induction heating step of disc #1, obvious sparks were observed on the edge of the disc, which suggests the input energy is large enough to melt the sample at the edge. Therefore, the particular shape of the axial and radial distortions of disc #1 can be attributed to the strongest IH recipe applied. As for the other four discs, the radial distortion profiles demonstrate a similar convex pattern over the whole disc thickness (Z), with the maximum radius nearby the mid-thickness of the disc and the minimum radius at the upper or lower part of the lateral face display as shown in Fig. 11(b)–(e).

3.2.2. Distortion comparison between group I and II

Distortion as a function of input energy is plotted for both groups of samples in Fig. 12. Samples from both groups show a similar trend but distortions for group I are systematically higher than for group II. Therefore, it can be concluded that, under the same IH treatment, samples with lower initial hardness undergo more distortion than those with higher hardness. This result is in contrast to the hardening depth observation between these two groups, where the discs with 27 HRC (279 HV) initial hardness demonstrated smaller hardening depth than those with 43 HRC (423 HV). If distortions were only due to the transformation process, one would expect that the more regions transformed, the larger the resulting distortions. However, the comparison between the results from group I and group II show a different tendency. This means the phase transformation during the IH treatment is not the only factor that can affect the distortion results.

3.3. Residual stress results

3.3.1. Stress-free lattice spacing d_0 results

Fig. 13 shows the stress-free lattice spacing d_0 profiles in the hoop and radial directions measured by ND on the reference (comb) sample. It is compared with the two d_0 values in radial direction measured from two thin (0.07 mm) layers of a similar sample by XRD.

The ND-measured d_0 in the hoop direction firstly demonstrates an increase near the surface, reaching a maximum of 1.1729Å ± 0.00016 followed by a diminishment with increasing depth through the hardened case and finally approaching a constant value of approximately 1.1715Å ± 0.00009 at a depth of around 2.0 mm. For the ND-measured d_0 in the radial direction, there is only a small variation in the stress-free lattice spacing near the surface followed by a smooth decrease towards the center and

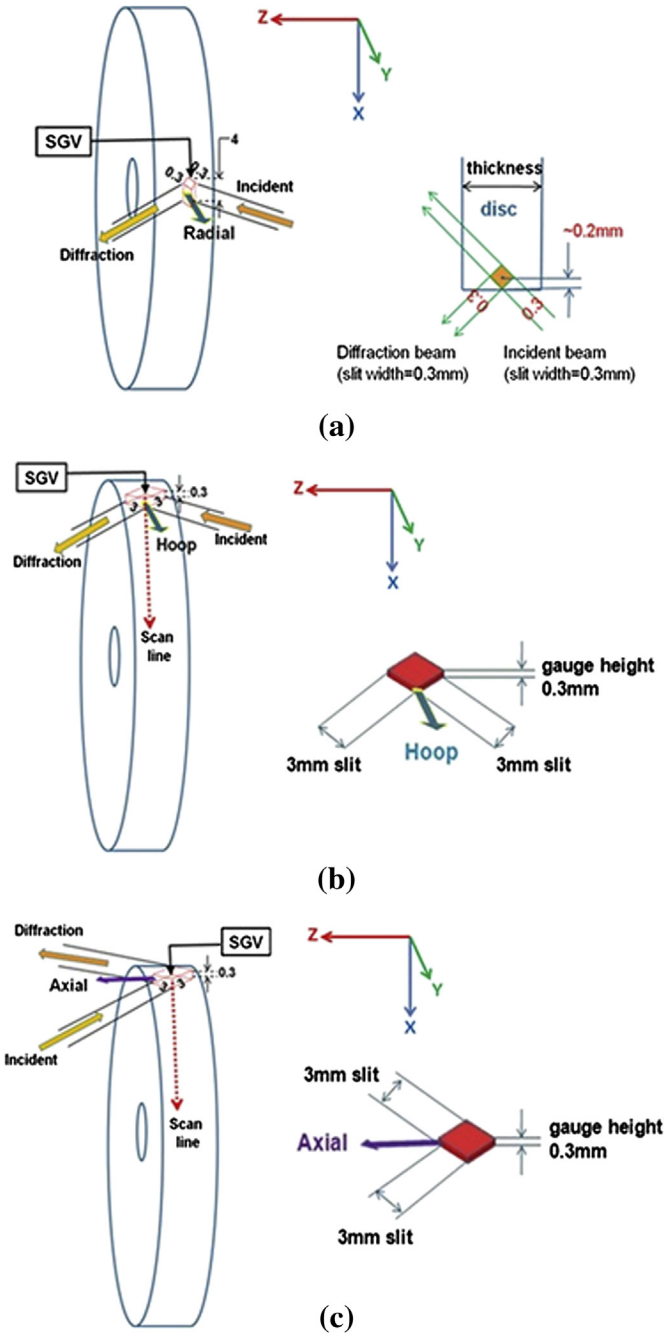

Fig. 7. SGV determinations in (a) radial, (b) hoop and (c) axial directions.

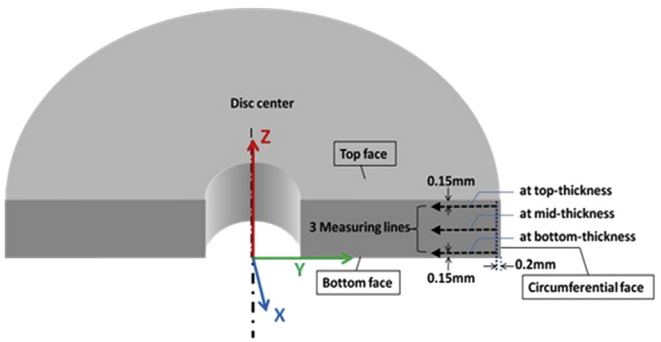

Fig. 8. Schematic sketch of the micro-hardness measurement path at three different thickness positions of the disc.

Please cite this article in press as: J. Yi, et al., Distortion and residual stress measurements of induction hardened AISI 4340 discs, Materials Chemistry and Physics (2013), http://dx.doi.org/10.1016/j.matchemphys.2013.07.012

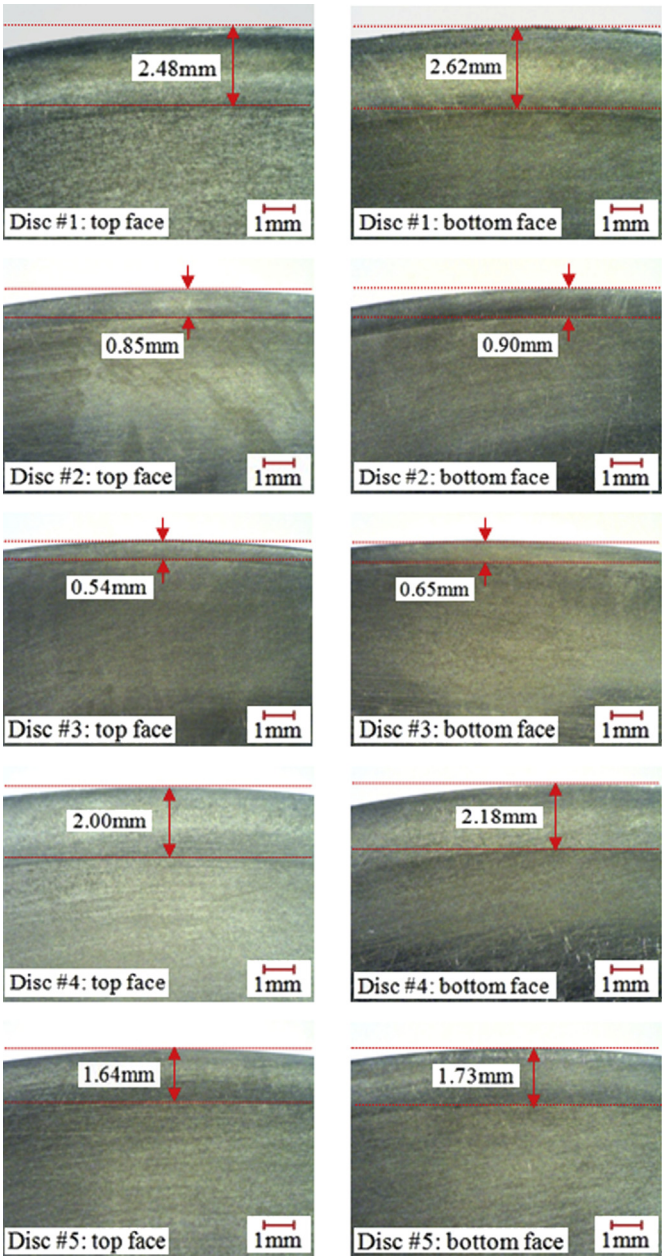

Fig. 9. Optical images showing the hardening depths: the left hand side is for the top surface of discs #1 to #5; the right hand side is for the bottom surface of discs #1 to #5.

reaching a constant value of approximately 1.1718Å ± 0.00013 at 2.2 mm.

Clearly, the ND-measured d_0 values in both directions (the hoop and radial directions) present a relatively higher value close to the surface than towards the core. This can be explained as the presence of carbon in solid solution in the martensite lattice leading to the increase of atomic spacing in the hardened layer. In the core region, since the material does not undergo any phase transformation during IH treatment, it keeps the original microstructure, the unstable tempered martensite. Therefore, the d_0 value in the core is relatively smaller than that in the hardened zone and nearly keeps a constant. Regarding the transition area, which has a mixed microstructure of fresh and over-tempered martensite, the corresponding d_0 value is consequently in between the one in the hardened and in the core region.

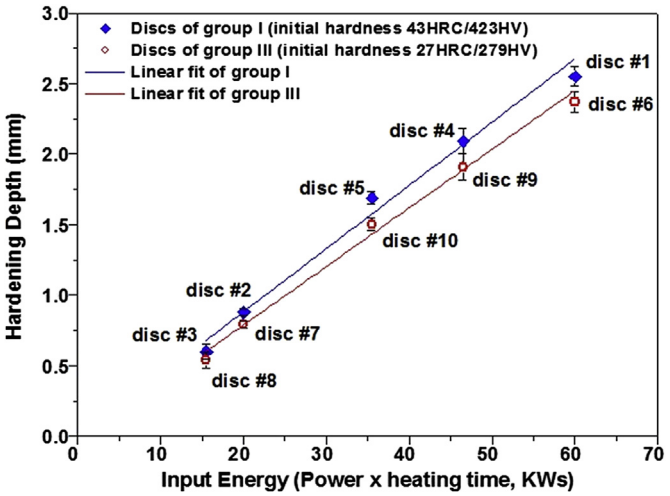

Fig. 10. Hardening depth comparison between group I with initial hardness of 43 HRC and group II with initial hardness of 27 HRC.

In order to make comparison, two XRD-determined d_0 values, the $d_{0-surface}$ of 1.17195Å ± 0.0001 and the d_{0-core} of 1.17079Å ± 0.0001, are indicated by two dashed lines in Fig. 13. These two d_0 values were measured from two thin (0.07 mm) sheets located at a depth of 0.6 mm and 20 mm below the free surface of a backup sample of disc #5. Obviously, the XRD results are in agreement with the ND outcome. The d_0 has a larger value in the hardened layer than in the core. A Comparison was made between the two ND-determined d_0 profiles and two d_0 values measured by XRD. It can be seen that the XRD-determined $d_{0-surface}$ is close to the ND-determined d_0 in the hardened layer. However, a clear discrepancy was found in the core material, where the XRD-determined d_{0-core} is significantly smaller than that measured by ND. The possible reasons for this discrepancy can be viewed from two aspects. Firstly, the reference comb sample used for ND d_0 determination may not be completely stress relieved, which results in inaccurate measurement. Considering that the tooth of the comb is very tiny, it is hard to perfectly machine each tooth in spite of using the wire-EDM cutting. Few teeth located in the core region were even bent to some extent, which implies a certain amount of residual stress may exist in those teeth. Secondly, there are experimental uncertainties in both ND and XRD measurements. For the d_0 investigation by ND, the uncertainty is mainly due to the fact that the number of counts (neutrons) detected for the diffraction peak formation is restricted by the small dimensions of the tiny teeth. This means, for each tooth, the amount of counts received by the detector may not be sufficient enough to give a very representative peak shape. Consequently, the center of the diffraction peak (used to calculate d_0) can vary within a small range and therefore the d_0 values may not be very representative at certain locations, especially the ones located in the core region where the bent teeth were observed. For the d_0 investigation by XRD, however, the main uncertainty is considered from the measuring system itself.

Since the d_0 values determined by ND display a certain amount of uncertainties, the d_0 investigating along the axial direction is not very necessary. The average value of d_0 in radial and hoop direction was therefore used as the d_0 value in axial direction to calculate the residual stress in corresponding direction.

3.3.2. Residual stress results

Fig. 14 demonstrates the residual stress distribution of the targeted disc in the hoop, axial and radial directions calculated based

Please cite this article in press as: J. Yi, et al., Distortion and residual stress measurements of induction hardened AISI 4340 discs, Materials Chemistry and Physics (2013), http://dx.doi.org/10.1016/j.matchemphys.2013.07.012

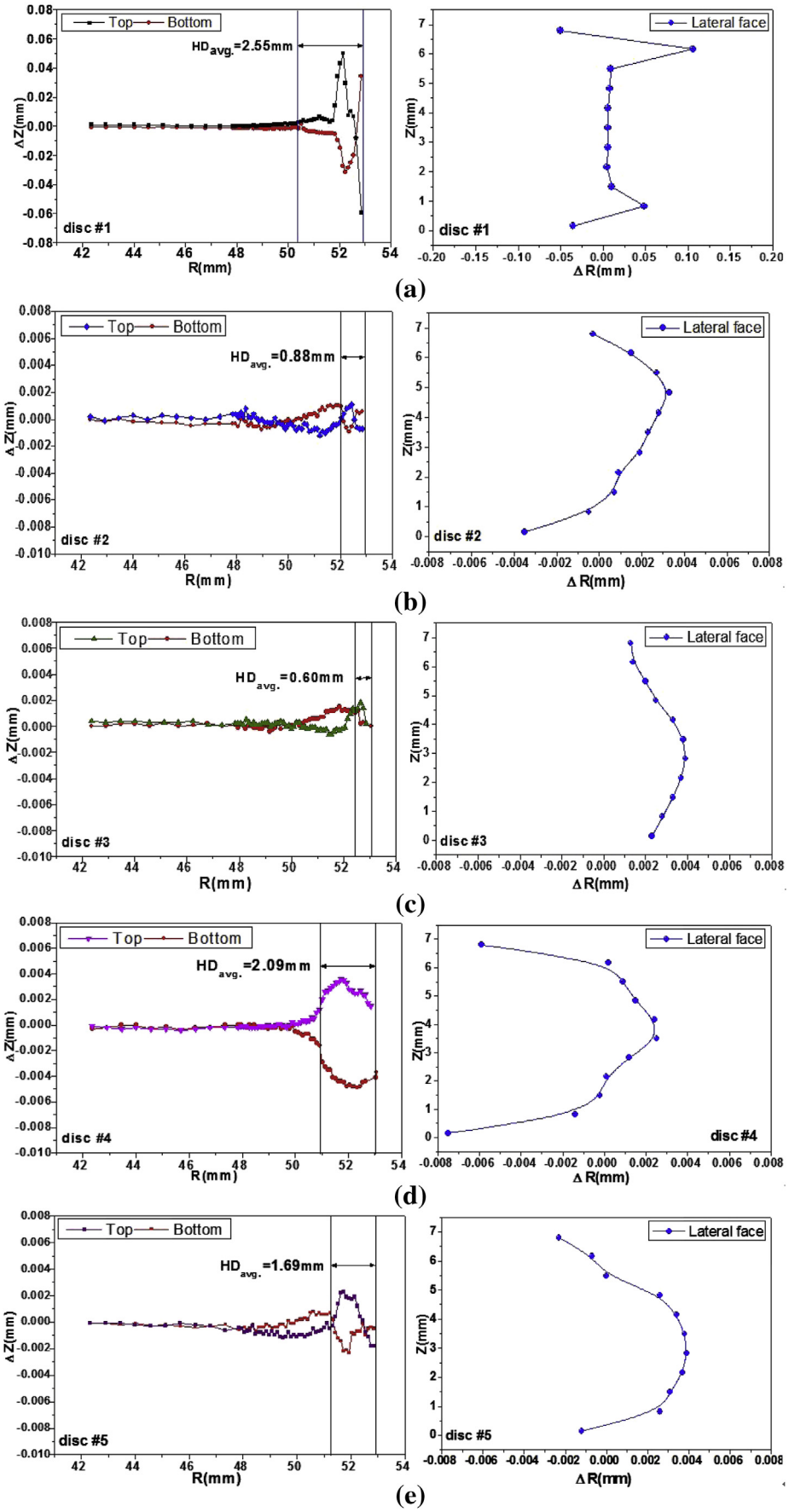

Fig. 11. IH distortion results of group I: (a) to (e) represent the axial distortion ΔZ (the left column) on the top/bottom face along radius of disc #1 to #5, and the radial distortion ΔR (the right column) on the lateral face along thickness of disc #1 to #5.

Please cite this article in press as: J. Yi, et al., Distortion and residual stress measurements of induction hardened AISI 4340 discs, Materials Chemistry and Physics (2013), http://dx.doi.org/10.1016/j.matchemphys.2013.07.012

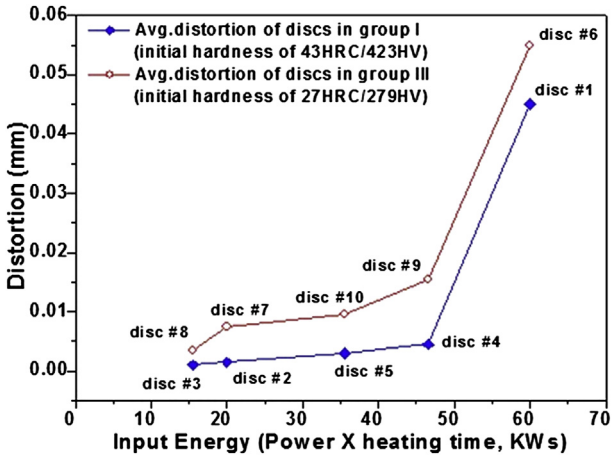

Fig. 12. Comparison between group I and II: distortions as a function of input energy.

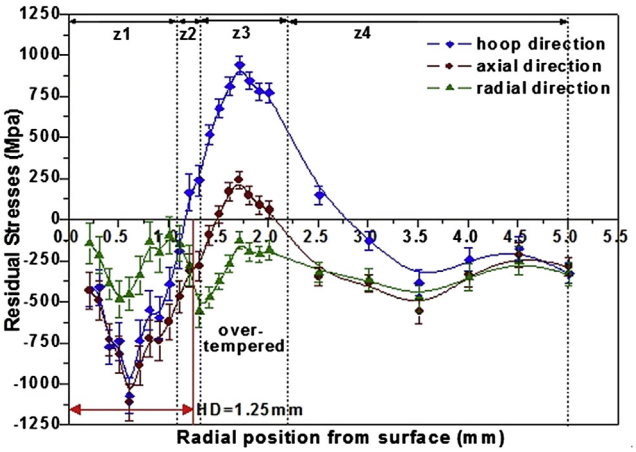

Fig. 14. Residual stress distribution in three directions calculated based on ND-measured d_0.

on the ND-measured d_0 profiles. Hoop and radial stresses were obtained from d_0 profiles in hoop and radial directions, respectively.

As can be seen from Fig. 14, a compressive residual stress field in the hoop and axial directions exists in the area close to the surface. This is similar to the work of Coupard et al. [9] and Hornbach et al. [17]. A reversal into tensile stress happens at the radial depth of 1.2 mm from the surface in hoop direction and 1.5 mm in axial direction. The maximum compressive stress in the hoop and axial directions are of the order of −1120 MPa, and they are observed at the same radial position (~0.65 mm) from the surface. A maximum tensile stress is found in hoop direction with an approximate value of 930 MPa. On the other hand, the axial stress is much smaller only 250 MPa. It implies that the hoop direction of the disc encountered the most critical stress condition (largest tensile stress), which is consistent with the most heat-treated cylindrical samples reported in the literature [18,19].

In addition, the radial stress is generally expected to be zero at the surface and the remaining radial (pseudo-normal) stresses are expected to be low due to the force balance requirement [20] considering the geometry of the sample. It is supported by literature which the heat-treated radial stress profiles show an almost constant value close to zero or only showing a slight variation over the whole radial direction [21]. In the present ND study, the radial stress is found to be compressive at the surface and demonstrates considerable variations along the radial positions within 2 mm from the surface. This finding is somewhat puzzling and is in contradiction with the relevant results obtained by Coupard et al. [9] and Prevey et al. [13]. Only Hornbach et al. [17] reported large variation in radial residual stress for induction hardened gear using XRD. Nevertheless, this obvious variation in radial direction can be somewhat related to the noticeable experimental errors and uncertainties observed in d_0 measurements (Fig. 13). Since the residual stress calculation is based on the reference d_0 value, the larger the possible error and uncertainty, the higher the effects on the residual stress value. Moreover, the ND experiment itself has certain uncertainties [11], especially at the region where phase transformation occurred (i.e. the near-surface area in the present study).

It is interesting to see that after 2.5 mm from the surface, the three stress profiles gradually merge and nearly coincide at the radial depth of around 5.0 mm at −250 MPa. It probably insinuates the beginning of the non-affected core region of the sample. However, the three component residual stresses should be all approaching to zero in the core material according to the principle of surface hardening stress distribution [22], which has been proved by numerous experimental works (e.g. the radial residual stress depth profile measured by ND [23] and XRD [24]). Therefore, the present constant stress value of about −250 MPa in the core should also be considered as an error which could be attributed to the corresponding uncertainty and errors existed in stress-free d_0 measurement such as being not 100% stress-free specimens.

If one uses the $d_{0-surface}$ and d_{0-core} measured by XRD to re-calculate the residual stress in these three directions, the overall profiles have shifted up and the results become more balanced in the core material (Fig. 15).

This observation is easy to be understood from Fig. 13 because the two XRD-determined d_0 values are relatively smaller than that obtained by ND, therefore the corresponding stress profiles in Fig. 15 move upwards. However, comparing Fig. 15 with Fig. 14 in terms of core region, it seems that at the depth relatively far from the surface the d_{0-core} measured by XRD may be closer to the real stress-free lattice spacing of the sample. The most reasonable explanation for this could be that the d_{0-core} measured by XRD on the thin layer is more reliable than the d_0 values obtained by ND (considering the significant uncertainty and error of d_0 measurements in the core region). Nevertheless, in terms of surface and phase transition areas, although the uncertainty of ND is relatively large, the d_0 profiles obtained by ND are more reliable. Since d_0 values should vary with the distance due to the phase

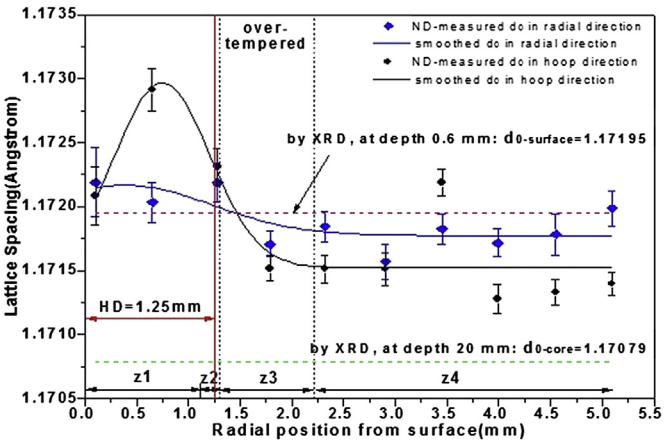

Fig. 13. {112} Radial and hoop stress-free lattice spacing (d_0) distributions along disc radius, determined from the comb specimen.

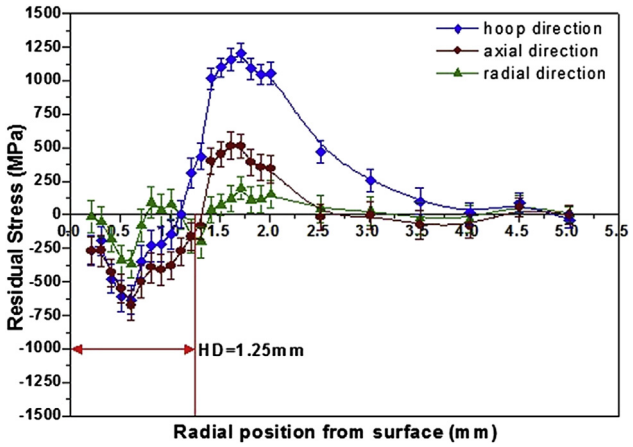

Fig. 15. Residual stress distribution in three directions calculated based on $d_{0-surface}$ and d_{0-core} measured by XRD.

transformation occurred during the IH surface treatment, it is much better to use the ND d_0 profile to analyze the case rather than using only one value $d_{0-surface}$.

Consequently, a 3-dimensional residual stress distribution by a combination of applying the ND-measured d_0 profiles in the surface region and the XRD-measured d_{0-core} in the core area is given in Fig. 16. Comparing Fig. 16 with Figs. 14 and 15, it is noted that the three stress profiles shown in Fig. 16 is a combination of that in Fig. 14 (in the surface and transition area) and in Fig. 15 (in the core region). Stress profiles demonstrate a near constant value (approaching to zero) in the core material while display a large compressive residual stress value in the surface hardened layer. In present study, Fig. 16 is more reasonable and may reflect the real case.

3.4. Micro-hardness results

Micro-hardness profiles for the targeted disc after induction hardening through three positions of top-, mid- and bottom-thickness as specified earlier are shown in Fig. 17(a). The corresponding vertical cross-section view of the hardening depth contour across the thickness of the disc is shown in Fig. 17(b).

It has been observed from Fig. 17(a) that the micro-hardness distributions along radial directions measured at mid-thickness,

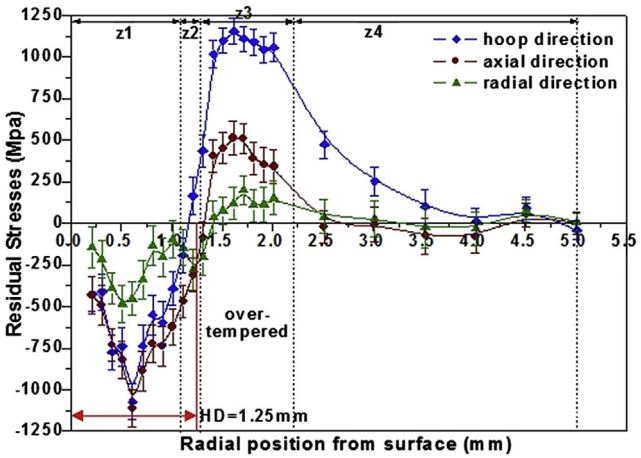

Fig. 16. Residual stress distribution in three directions calculated based on ND-measured d_0 for the surface area and the d_{0-core} obtained by XRD for the core material.

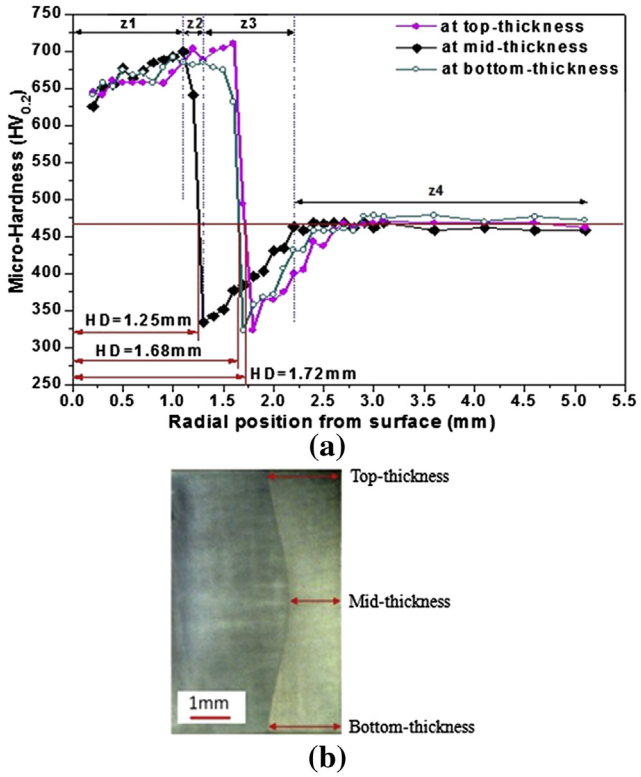

Fig. 17. (a) Micro-hardness profiles of the disc, measured through the top-, mid- and bottom-thickness positions; (b) vertical cross-section view of the hardening depth contour across the thickness of the disc.

top-thickness and bottom-thickness have similar trends. As shown, all three curves demonstrate a typically high hardness value varying from 625 $HV_{0.2}$ to 700 $HV_{0.2}$ near the surface. This region of high hardness is called the hardened zone and is quantified by the depth z1 as displayed in Fig. 17. This region is followed by a sharp decrease until reaching a minimum around 320 $HV_{0.2}$, indicating a transition zone (which size is z2). From that minimum value, the hardness gradually goes up progressively to reach the core hardness (470 $HV_{0.2}$), forming the over-tempered zone (z3). Afterwards, the hardness keeps a nearly constant value around 470 $HV_{0.2}$ in the core material, which is the same value as the initial hardness before induction hardening and therefore reveals the non-affected zone (z4).

The slight increasing trend in the hardness of the surface hardened layer with moving towards the center was also observed by Grum [25]. This could be explained by the formation of a very fine martensitic microstructure in the inner region of the hardened layer due to the non-uniform cooling rates in the disc surface during the IH process. The “groove” in the hardness profile, in the over-tempered zone (z3) is a fairly common feature when tempered martensite is subjected to IH. This is due to the tempering effect of the thermal flow happening during the IH treatment. More detailed study on the entire hardness profile especially the over-tempered zone of the induction hardened specimen was reported by Ducassy [26].

Analyzing the hardening depth at the mid-, top- and bottom-thickness, a distinct difference has been noted. In the present study, the hardening depth is defined as the radial position in region z2 where the hardness reaches the core hardness. The value of hardening depth measured at top-thickness and bottom-thickness are very close to each other (around 1.6–1.7 mm) and they are also similar to the estimated hardening depth value obtained by image

Please cite this article in press as: J. Yi, et al., Distortion and residual stress measurements of induction hardened AISI 4340 discs, Materials Chemistry and Physics (2013), http://dx.doi.org/10.1016/j.matchemphys.2013.07.012

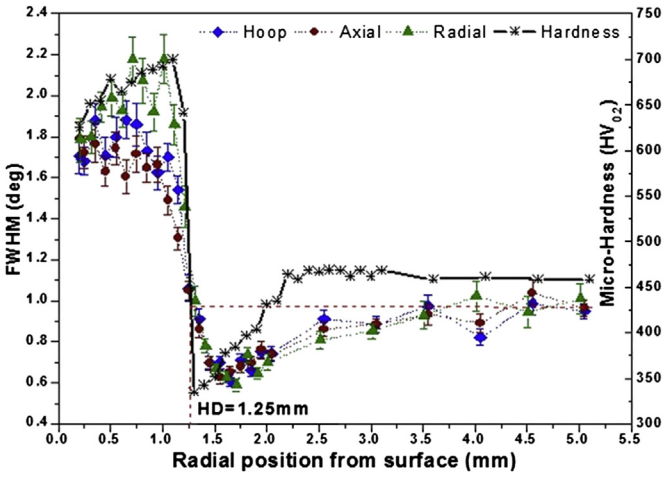

Fig. 18. *Fe{112}* diffraction peak FWHM distributions along radius.

analysis (as described in Section 2.5, using optical microscopy). In Fig. 17(b), the red arrows indicate the hardening depth at the top-, mid- and bottom-thickness of the disc. However, they are obviously larger than the mid-thickness hardening depth, which is only 1.2 mm, leading to a clear and characteristic hardened case profile has been exposed with a convex shape towards the lateral face (Fig. 17(a)). This variation in the hardening depth at different positions has been viewed as a result of the edge effect caused by the concentration of the magnetic field at the disc edges [27].

If one compares the residual stress profile with the hardness profile (Fig. 17(a)), a sharp transition area can be observed in both profiles at a similar location, suggesting that the tendency of compressive residual stress profile is in accord with the trend of the corresponding hardness profile. This finding is further supported by the work of Grum [25] stating that a steeper reduction in hardness may contribute a sharp change of residual stress. Moreover, with respect to the radial positions after 2.5 mm, both the hardness distribution and the three residual stress profiles show a consistent trend. They actually approach to a nearly constant value towards the core around the same depth value (3 mm).

3.5. Full width half maximum (FWHM) results

The FWHM profile of the *Fe{112}* $K\alpha_1$ diffraction peak is illustrated in Fig. 18. The relevant hardness curve is also given for better explanation. As seen, the overall FWHM profile in the hoop, axial and radial directions are quite similar. The only noticeable difference in peak width among them appears within the hardened layer. Regarding the transition zone and core material region, the three FWHM curves are very close to each other even overlapping at many radial positions. Besides, all the three FWHM profiles display a visible variation in the hardened region up to a radial depth around 1.0 mm below the surface, and such variations could be related to the likewise hardness fluctuation in surface hardened region, suggesting the inhomogeneous microstructure generated in the surface layer, possibly caused by the dislocations in the hardened layer.

Moreover, after the hardened region, the peak width declines quickly towards the center until reaching a minimum value around 0.6° at a radial depth of 1.5 mm, approximately. This is closely followed by a gradual increase to approach a nearly constant value of 1.0°, revealing the core material zone. The remarkable trough appeared in the FWHM curve is consistent with the similar groove

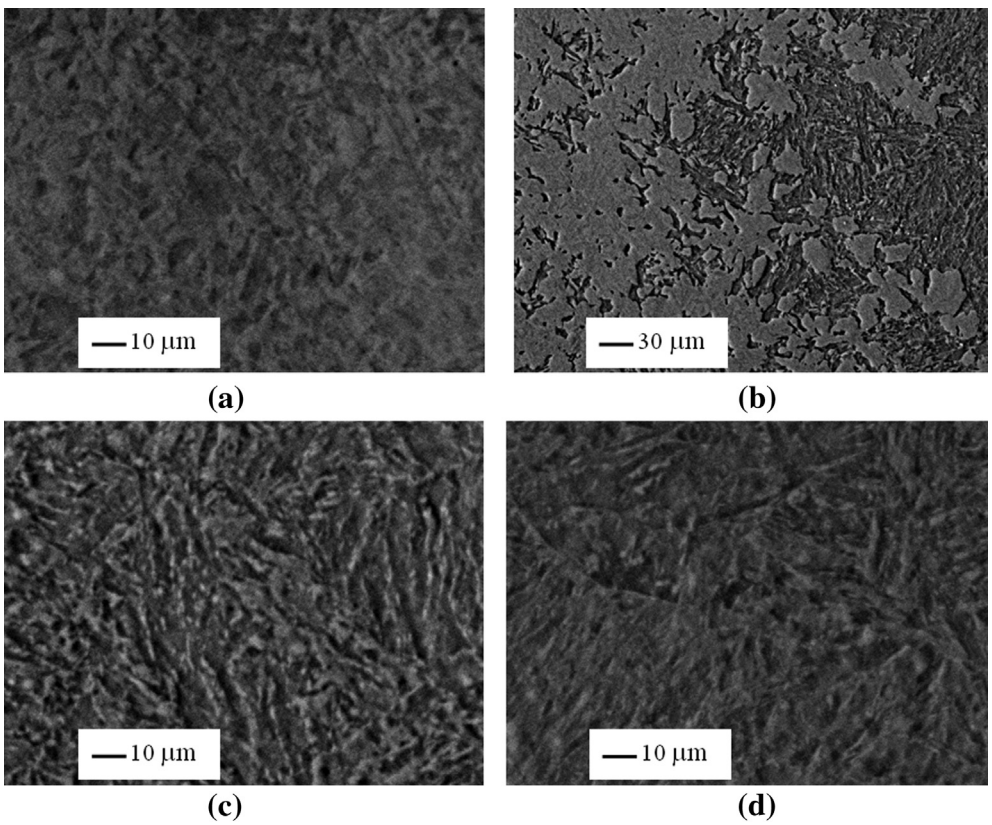

Fig. 19. Microstructures over the cross-section of disc #5: (a) hardened region; (b) transition region; (c) over-tempered region; (d) non-affected region.

Please cite this article in press as: J. Yi, et al., Distortion and residual stress measurements of induction hardened AISI 4340 discs, Materials Chemistry and Physics (2013), http://dx.doi.org/10.1016/j.matchemphys.2013.07.012

pattern found in the hardness profile (Fig. 17(a)), which could be seen as the material over-tempering nature taking place at the end of the hardened region.

3.6. Microstructure results

The corresponding SEM microstructural analysis of the cross-section of disc #5 is given in Fig. 19. Fig. 19(a)–(d) represents the microstructure of hardened zone (z1), transition zone or otherwise called hardness loss zone (z2), over-tempered zone (z3) and non-affected core zone (z4).

It can be seen from Fig. 19(a) that the microstructure in the hardened zone is completely hard martensite. This is because the heating temperature in this area is above Ac3 and based on the fast cooling, the microstructure can be completely transformed from austenite to martensite. A mixed microstructure of hard martensite and over-tempered martensite is observed in Fig. 19(b), since the temperature in the transition zone is between Ac1 and Ac3. Fig. 19(c) displays a completely over-tempered martensite microstructure. In this region, the corresponding temperature is still high (due to the heat flow effect), but without reaching the critical point Ac1, the material is only tempered without being austenitized. It finally transforms to a more stable state (i.e., ferrite with dispersed carbides) which is associated with a loss of hardness, as can be seen from the groove in the hardness profile in Fig. 17(a). Fig. 19(d) displays the microstructure of the core of the disc. It is composed of the initial microstructure (the quenched and tempered martensite) of the sample without being affected by the IH treatment. Also, one may observe directly from Fig. 19(c) that the over-tempered martensite microstructure seems to be more disordered compared with that in the hardened and core region.

Moreover, since the tempered martensite has larger grain size than the quenched one, it can be understood that the grain size in the over-tempered region is larger than that in the core area and followed by the hardened zone. Therefore, the FWHM plot demonstrates a drop from surface to core and has a groove in the over-tempered zone, considering the Scherrer formula (FWHM $\sim 1/d$) [11].

4. Conclusions

The present study shows that both the IH parameters (heating time and input power) and the initial hardness affect the distortion and hardening depth of the samples. Under the same initial hardness, increasing IH parameters (heating time or input power) increase both the hardening depth and distortions of the disc. However, under the same IH parameters, increasing the initial hardness of the disc increases the hardening depth as it decreases the distortions of the disc.

Due to the severe variations of the hardness at the surface of a IH part, the knowledge of d_0 depth distribution is necessary and it can significantly affect the residual stress results. A variation of 0.001Å in d_0 in hardened layer can result a difference in residual stress around 200 MPa in the same region. Both ND- and XRD-measured d_0 results display a visible difference in d_0 values between hardened layer and core material. Therefore, it is more reasonable to apply ND-measured d_0 profile to calculate the residual stress near the surface than using a constant $d_{0-\text{surface}}$ value measured by XRD. However, for the core material, the XRD-measured $d_{0-\text{core}}$ is more reliable. The final residual stress distributions are constructed based on the combination of ND and XRD d_0 results.

Acknowledgment

The authors thank Benjamin Larregain from helping with the induction hardening treatments and Antoine Faure for the development of the distortion measurement procedure on present and Majid Hoseini for his help in d_0 measurements by XRD.

References

[1] R.E. Haimbaugh, Practical Induction Heat Treating, ASM International, Materials Park, OH, 2001, pp. 5–18.
[2] H. Kristoffersen, P. Vomacka, Mater. Des. 22 (2001) 637–644.
[3] D.H. Xu, Z.B. Kuang, J. Eng. Mat. Tech. 118 (1996) 571–575.
[4] K.A. Young, Machining-induced Residual Stress and Distortion of Thin Parts. Ph.D. dissertation, Washington University, Saint Louis, MO, May 2005.
[5] C.O. Ruud, NDT Int. 15 (1982) 15–23.
[6] M.E. Hilley (Ed.), SAE, vol. 784, 1971, pp. 21–24.
[7] O. Kirstein, V. Luzin, A. Brule, H. Nguyen, D. Tawfik, Adv. Mater. Res. 41–42 (2008) 439–444.
[8] M.G. Moore, W.P. Ewans, SAE Trans. 66 (1958) 340.
[9] D. Coupard, T. Palin-luc, P. Bristiel, V. Ji, C. Dumas, Mater. Sci. Eng. A 487 (2008) 328–339.
[10] G.A. Webster, in: M.T. Hutchings, A.D. Krawitz (Eds.), Measurement of Residual and Applied Stress Using Neutron Diffraction, NATO ASI Series E, Kluwer Academic Publishers, Dordrecht, Netherlands, 1992, pp. 21–36.
[11] M.T. Hutchings, P.J. Withers, T.M. Holden, T. Lorentzen, Introduction to the Characterization of Residual Stress by Neutron Diffraction, Taylor & Francis, Boca Raton, FL, 2005.
[12] P.S. Prevey, in: C. Ruud (Ed.), Practical Applications of Residual Stress Technology, ASM, Materials Park, OH, 1991, pp. 47–54.
[13] P.S. Prevey, P.W. Mason, in: C. Ruud (Ed.), Practical Application of Residual Stress Technology, ASM, Materials Park, OH, 1991, pp. 77–81.
[14] A.N. Ezeilo, G.A. Webster, P.J. Webster, M. Roth, W.J. Muster, in: Proceeding of 2nd European Conf. on Adv. Materials and Processes, Euromat 91, Cambridge, 1991, pp. 389–394.
[15] Alloy Digest, Steel-alloy Collection (ASM International 2002). AISI-4340, Filing Code: SA-14, Feb. 1954.
[16] C.A. Siebert, D.V. Doane, D.H. Breen, The Hardenability of Steel: Concepts, Metallurgical Influences, and Industrial Applications, ASM, Materials Park, 1977, pp. 162–178.
[17] D.J. Hornbach, P.S. Prevey, P.W. Mason, in: Proceeding of the 1st Int. Conf. on Induction Hardened Gears and Critical Components Gear Research Institute, Indianapolis, IN, 1995, pp. 69–76.
[18] M.B. Prime, V.C. Prantil, P. Rangaswamy, F.P. Garcia, Mater. Sci. Forum 347–349 (2000) 223–228.
[19] G.E. Totten, N.I. Kobasko, L.C.F. Canale, in: MECOM 2005-VIII Congreso Argentino de Mecanica Computacional, Buenos Aires, Argentina, 2005, pp. 1041–1058.
[20] A. Payzant, S. Spooner, X.J. Zhu, C.R. Hubbard, in: ASME Pressure Vessels and Piping Conference, MTL, Canada, 1996, pp. 21–26.
[21] G. Albertini, et al., Physica B 276–278 (2000) 925–926.
[22] P.J. Withers, H.K.D.H. Bhadeshia, Mater. Sci. Technol. 17 (2001) 355–365.
[23] M.A. Wells, B.H.- Morales, J.H. Root, E.B. Hawbolt, Physica B 241–243 (1998) 1274–1276.
[24] P.M.C.L. Pacheco, M.A. Savi, A.F. Camarão, J. Strain Anal. 36 (2001) 507–512.
[25] J. Grum, J. Mater. Process. Technol. 114 (2001) 212–226.
[26] C. Ducassy, Prediction de la durete et de la profondeur de la zone de sur-revenu lors d'une chauffe rapide par induction d'un acier 4340 trempe revenu. M. Ing. Thesis, Ecole de Technologie Superieure, Montreal, QC, Canada, 2010.
[27] N. Barka, A. Chebak, J. Brousseau, Study of edge effect of 4340 steel specimen heated by induction process using axi-symmetric simulation, in: Proceedings of the Progress in Electromagnetics Research Symposium, Marrakesh, Morocco, Mar, 2011, pp. 1207–1203.

Please cite this article in press as: J. Yi, et al., Distortion and residual stress measurements of induction hardened AISI 4340 discs, Materials Chemistry and Physics (2013), http://dx.doi.org/10.1016/j.matchemphys.2013.07.012